inorganics

MDPI

Supplementary Materials: Breast Cancer Stem Cell Active Copper(II) Complexes with Naphthol Schiff Base and Polypyridyl Ligands

Table of Content

Figure S26. Representative dose-response curves for the treatment of HMLER and HMLER-shEcad cells with **L**[3].

Figure S27. Bright-field images (taken using an inverted microscope) representative of untreated HMLER-shEcad mammospheres and those treated with salinomycin for 5 days at its IC_{20} values. Scale bar = 160 μm.

Figure S28. Bright-field images (taken using an inverted microscope) representative of untreated HMLER-shEcad mammospheres and those treated with **L**[2] or **L**[3] for 5 days at their respective IC_{20} values. Scale bar = 100 μm.

Figure S29. Representative dose-response curve for the treatment of HMLER-shEcad mammospheres with **2** after 5 days incubation.

Figure S30. Representative dose-response curve for the treatment of HMLER-shEcad mammospheres with **3** after 5 days incubation.

Figure S31. Representative dose-response curve for the treatment of HMLER-shEcad mammospheres with **4** after 5 days incubation.

Figure S32. Representative dose-response curve for the treatment of HMLER-shEcad mammospheres with **5** after 5 days incubation.

Figure S33. Representative dose-response curve for the treatment of HMLER-shEcad mammospheres with **L**[2] after 5 days incubation.

Figure S34. Representative dose-response curve for the treatment of HMLER-shEcad mammospheres with **L**[3] after 5 days incubation.

Figure S35. Normalised ROS activity in untreated HMLER-shEcad cells (control) and HMLER-shEcad cells treated with **2** (2 × IC_{50} value for 0.5, 1, 3 6, 16, and 24 h). Error bars represent standard deviations and Student *t test*, * = $p < 0.05$.

Figure S36. Normalised ROS activity in untreated HMLER-shEcad cells (control) and HMLER-shEcad cells treated with **3** (2 × IC_{50} value for 0.5, 1, 3 6, 16, and 24 h). Error bars represent standard deviations and Student *t test*, * = $p < 0.05$.

Figure S37. Normalised ROS activity in untreated HMLER-shEcad cells (control) and HMLER-shEcad cells treated with H_2O_2 (150 μM for 0.5, 1, 3 6, 16, and 24 h). Error bars represent standard deviations and Student *t test*, * = $p < 0.05$.

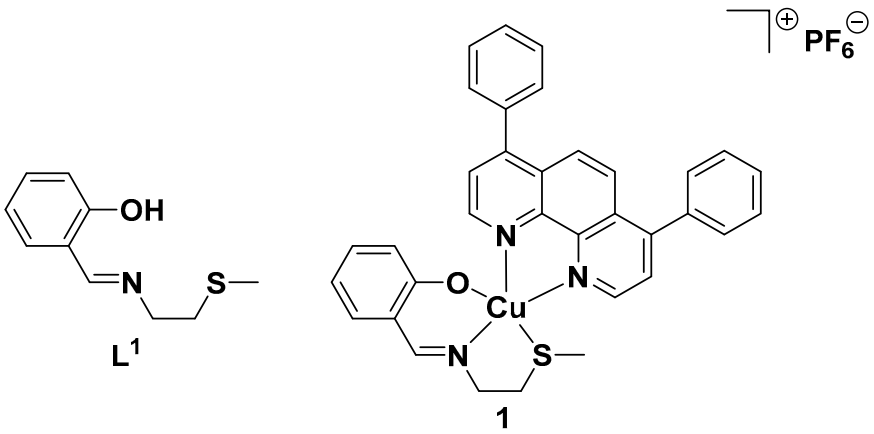

Figure S1. Chemical structures of the Schiff base ligand **L**[1] and the copper(II) complex **1** containing **L**[1] and 4,7-diphenyl-1,10-phenanthroline. The copper(II) complex **1** was previously shown by our group to kill breast cancer stem cells (CSCs) via cytotoxic and immunogenic mechanisms.

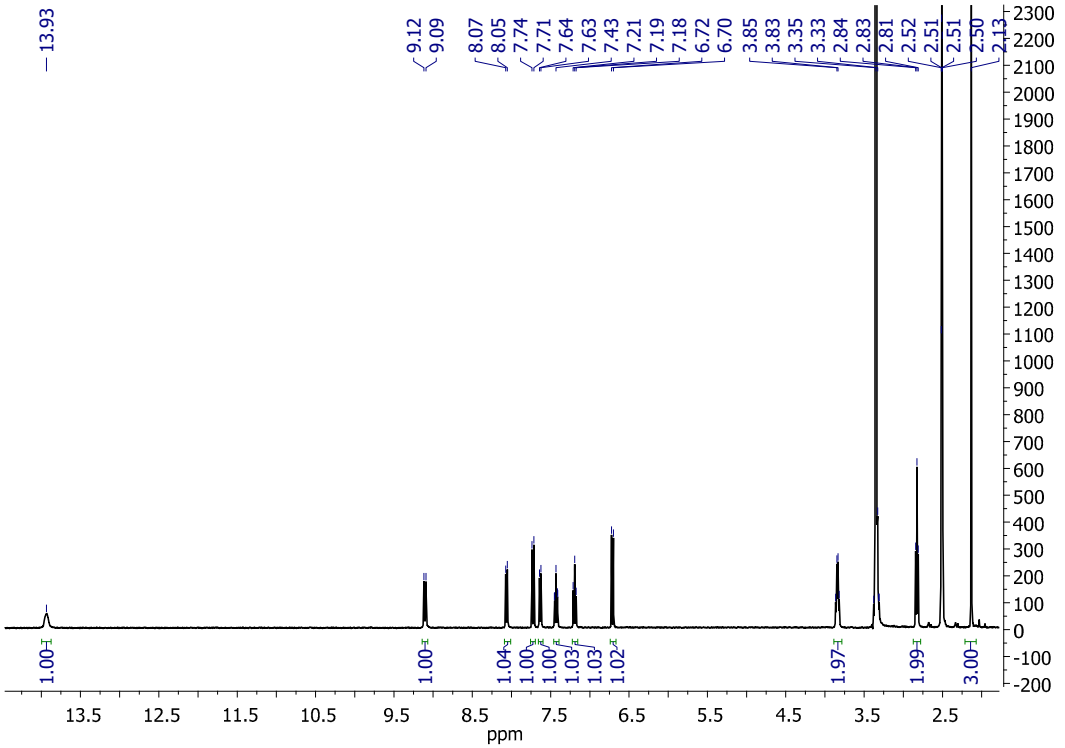

Figure S2. ^{1}H NMR spectrum of **L²** in DMSO-d$_6$.

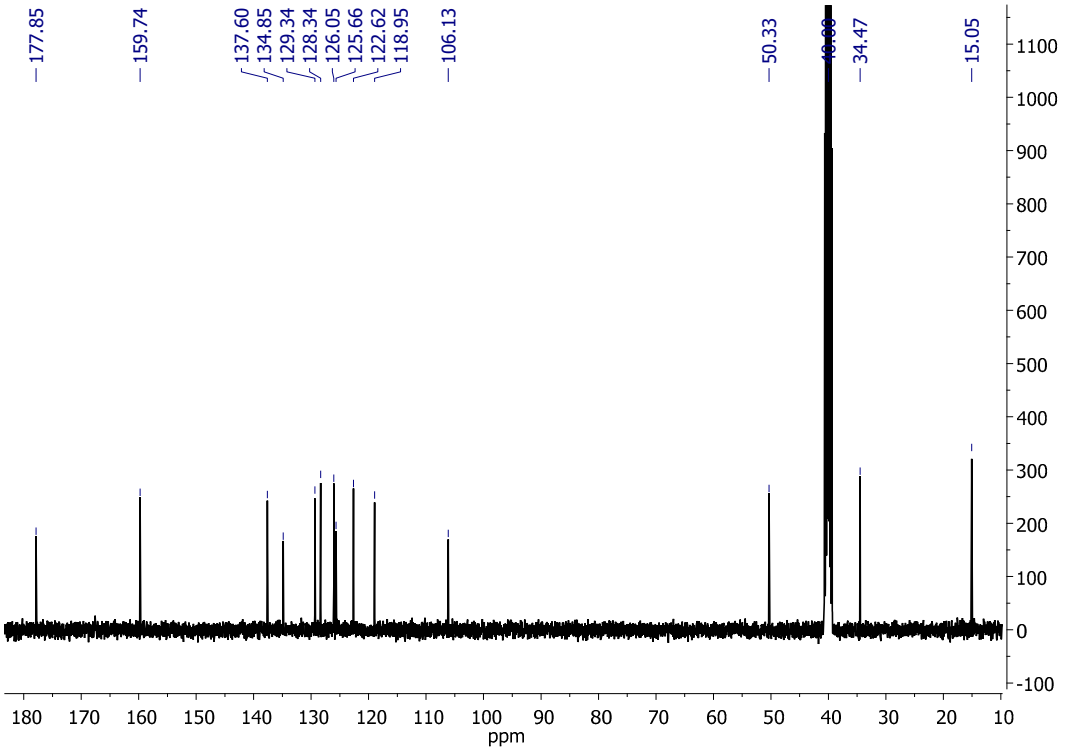

Figure S3. ^{13}C{^{1}H} NMR spectrum of **L²** in DMSO-d$_6$.

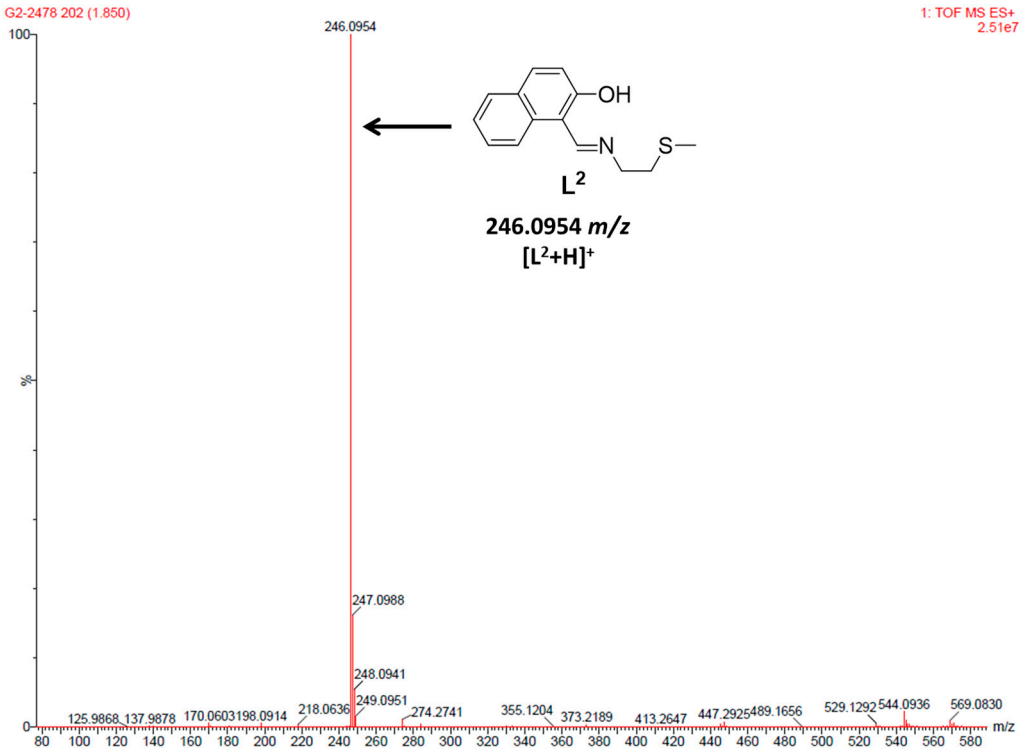

Figure S4. HR-ESI mass spectrum (positive mode) of **L²**.

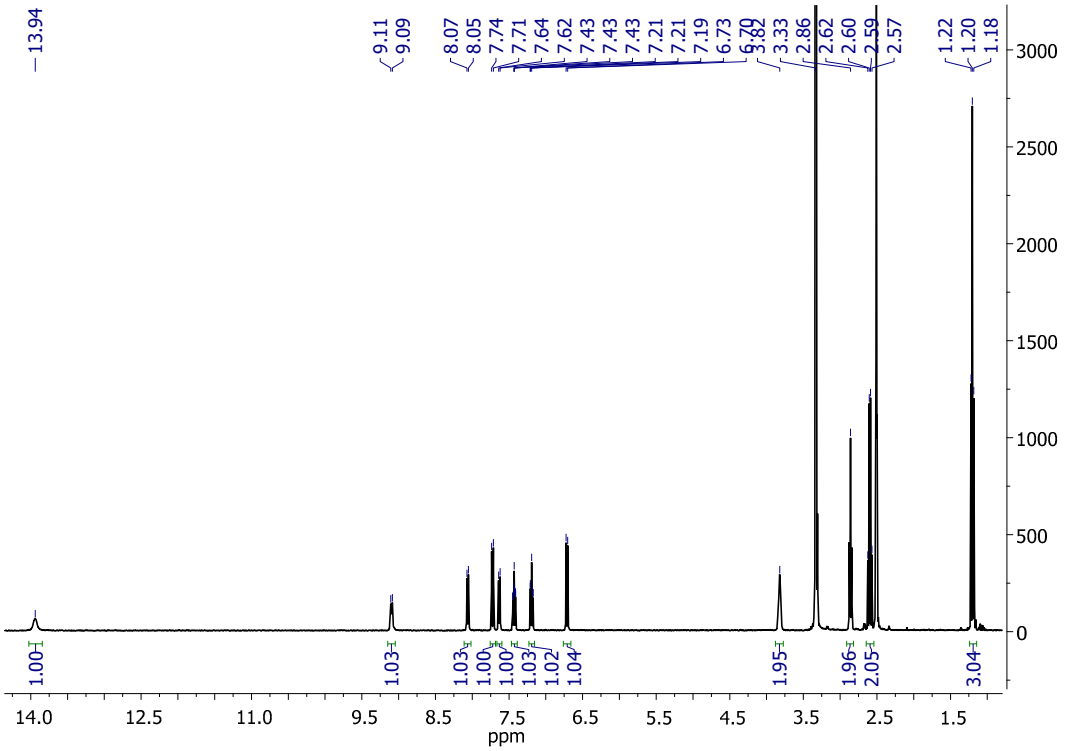

Figure S5. ^{1}H NMR spectrum of **L^{3}** in DMSO-d$_{6}$.

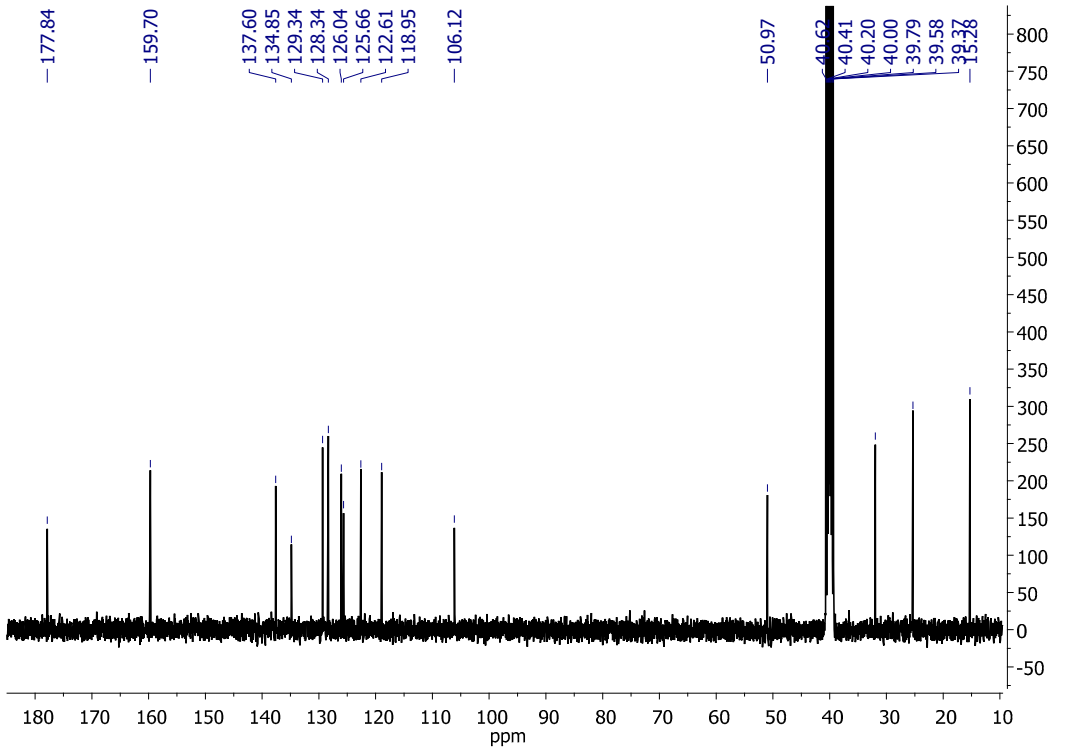

Figure S6. ^{13}C{^{1}H} NMR spectrum of **L^{3}** in DMSO-d$_{6}$.

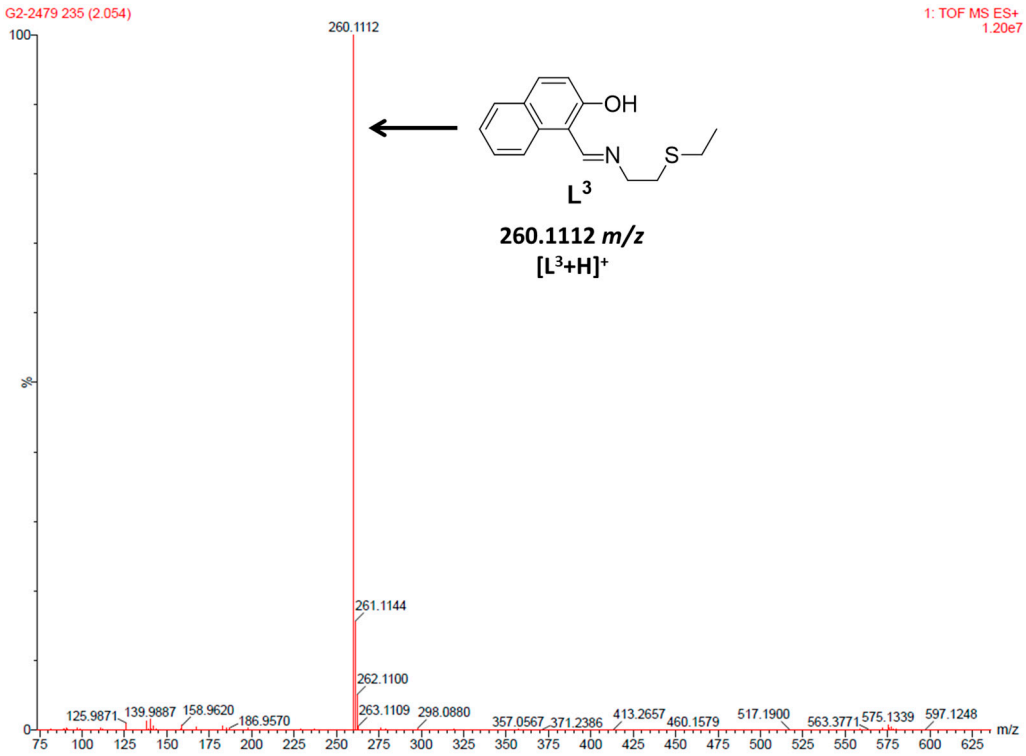

Figure S7. HR-ESI mass spectrum (positive mode) of **L**[3].

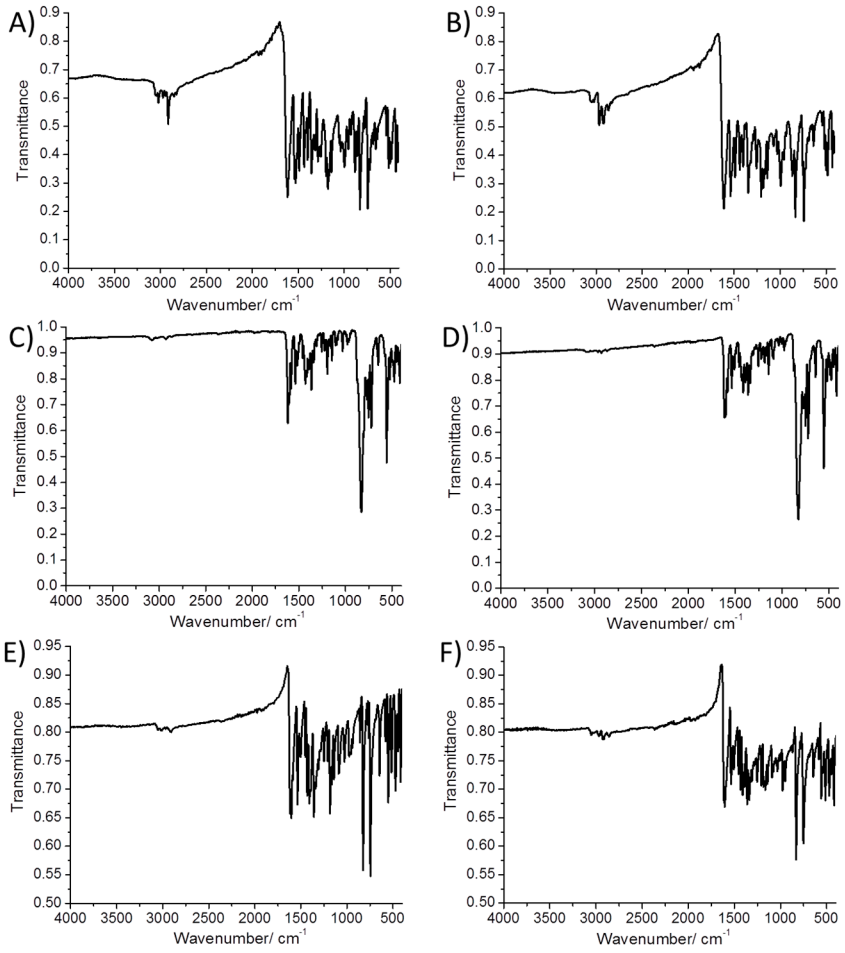

Figure S8. IR spectrum of (A) **L**[2], (B) **L**[3], (C) **2**, (D) **3**, (E) **4**, and (F) **5** in the solid form.

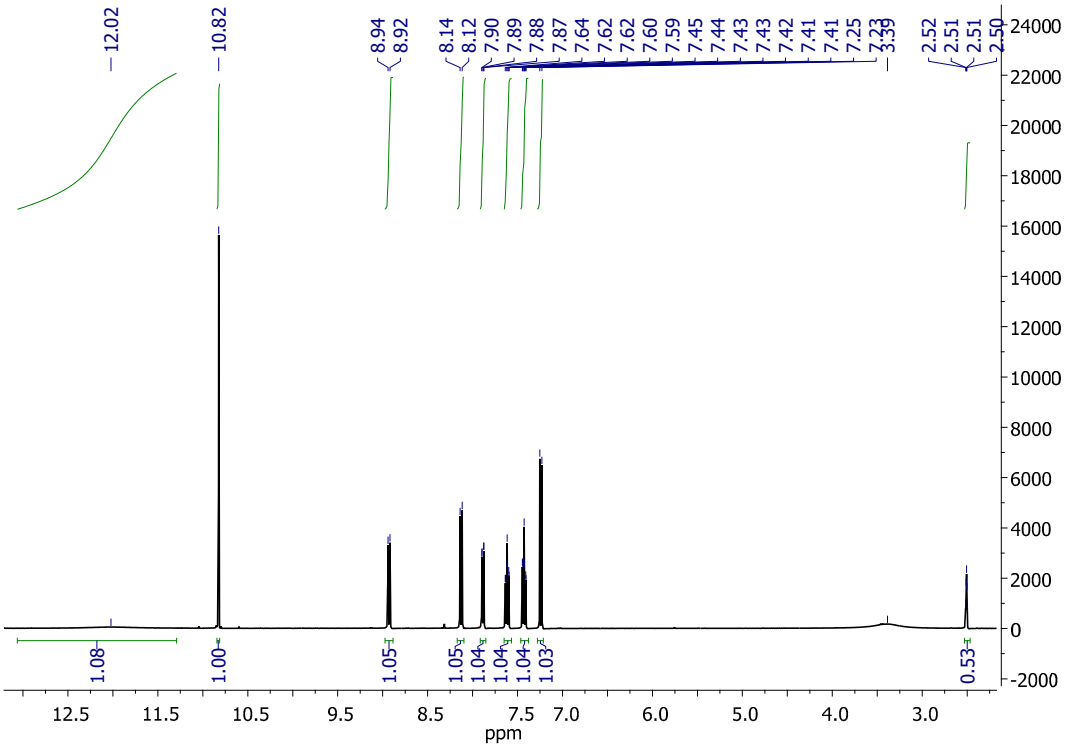

Figure S9. [1]H NMR spectrum of 2-hydroxy-1-naphthaldehyde in DMSO-d6.

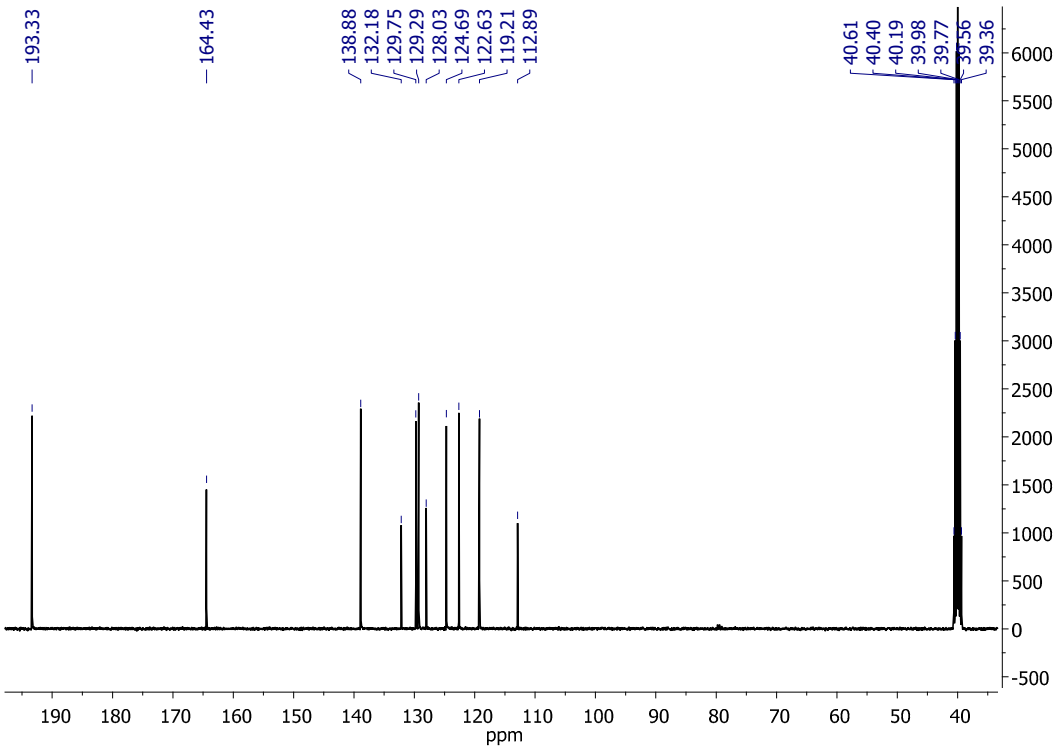

Figure S10. $^{13}C\{^{1}H\}$ NMR spectrum of 2-hydroxy-1-naphthaldehyde in DMSO-d_6.

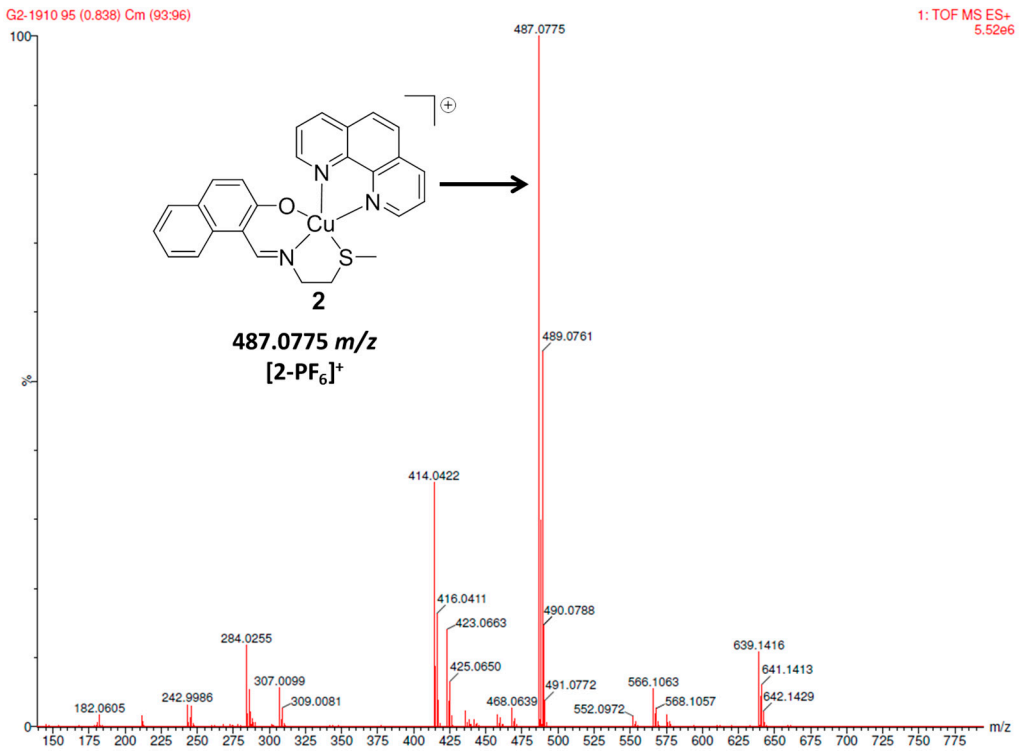

Figure S11. HR-ESI mass spectrum (positive mode) of **2**.

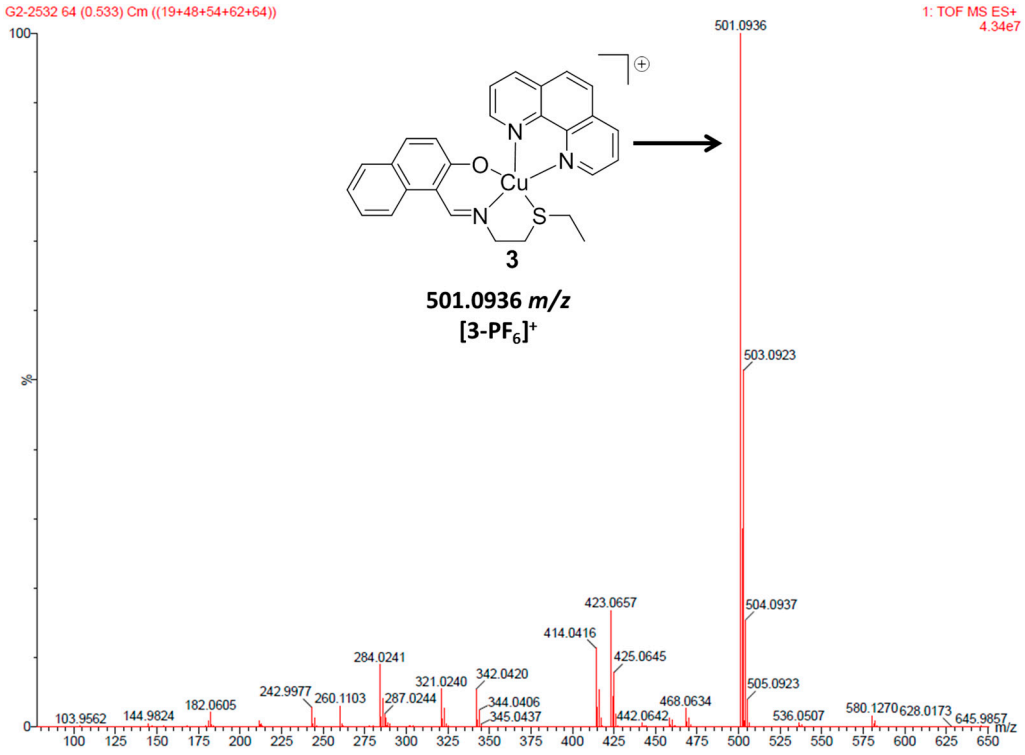

Figure S12. HR-ESI mass spectrum (positive mode) of **3**.

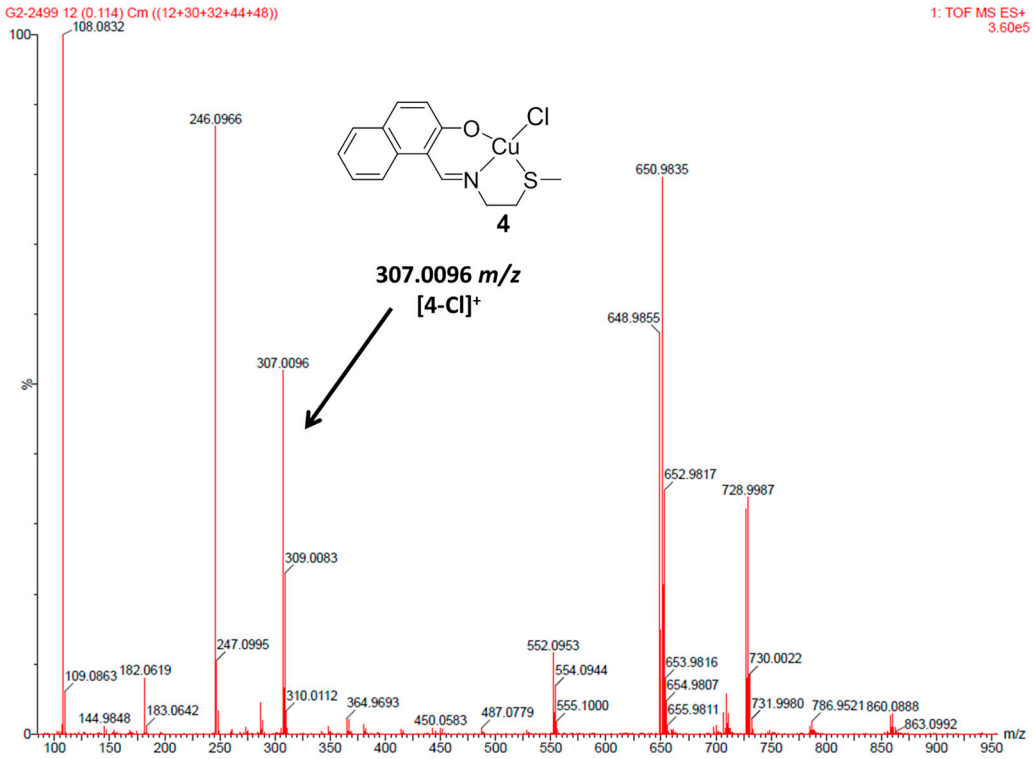

Figure S13. HR-ESI mass spectrum (positive mode) of **4**.

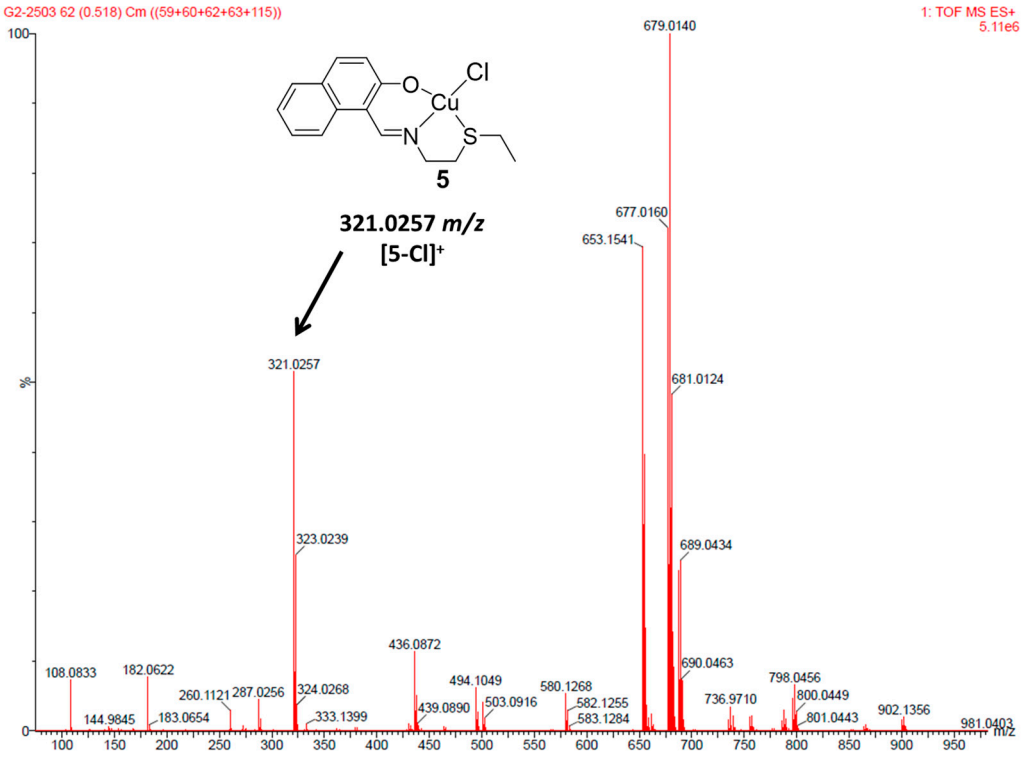

Figure S14. HR-ESI mass spectrum (positive mode) of **5**.

Table S1. Crystallographic data for **2** and **3**.

Metal complex	**2**	**3**
CCDC No.	2046680	2046679
formula	$C_{26}H_{22}N_3OF_6PSCu$	$C_{27}H_{24}CuF_6N_3OPS$
Fw	633.03	647.06
Crystal system	monoclinic	monoclinic
Space group	$P2_1/n$	$P2_1/c$
a, Å	13.926(3)	8.471(4)
b, Å	13.293(3)	17.550(9)
c, Å	14.251(3)	18.443(9)
α, deg.	90	90
β, deg.	97.527(4)	99.605(11)
γ, deg.	90	90
V, Å^3	2615.3(11)	2703(2)
Z	4	4
ϱ_{calc}g/cm^3	1.608	1.590
2θ / deg.	3.846 to 51.994	3.226 to 51.998
Reflections collected	19911	20967
Independent reflections	5119	5307
Goodness-of-fit on F^2	0.996	0.886
R_1, wR_2 [$I \geq 2\sigma$ (I)]	0.0545, 0.1193	0.0636, 0.1198
R_1, wR_2 [all data]	0.0788, 0.1282	0.1315, 0.1426
Largest diff. peak/hole / e Å^{-3}	0.59/-0.41	0.42/-0.40

Table S2. Selected bond lengths (Å) and angles (°) for **2**.

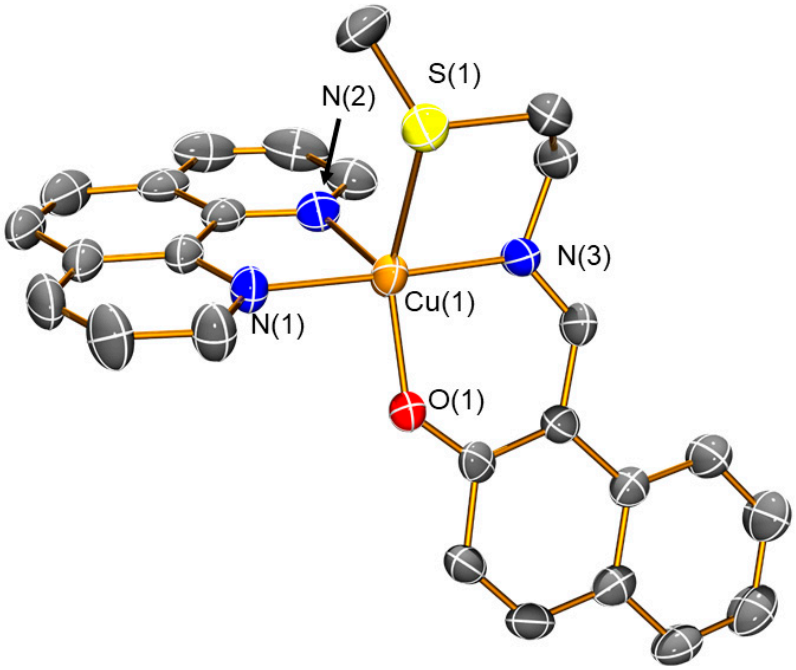

Cu(1)-S(1)	2.5220(11)	Cu(1)-N(2)	2.152(3)
Cu(1)-O(1)	1.908(2)	Cu(1)-N(3)	1.933(3)
Cu(1)-N(1)	2.007(3)		
O(1)-Cu(1)-S(1)	131.68(8)	N(2)-Cu(1)-S(1)	102.30(8)
O(1)-Cu(1)-N(1)	89.49(10)	N(3)-Cu(1)-S(1)	83.50(9)
O(1)-Cu(1)-N(2)	125.71(10)	N(3)-Cu(1)-N(1)	177.78(12)
O(1)-Cu(1)-N(3)	92.59(11)	N(3)-Cu(1)-N(2)	99.72(12)
N(1)-Cu(1)-S(1)	94.53(9)	N(1)-Cu(1)-N(2)	79.67(11)

Table S3. Selected bond lengths (Å) and angles (°) for **3**.

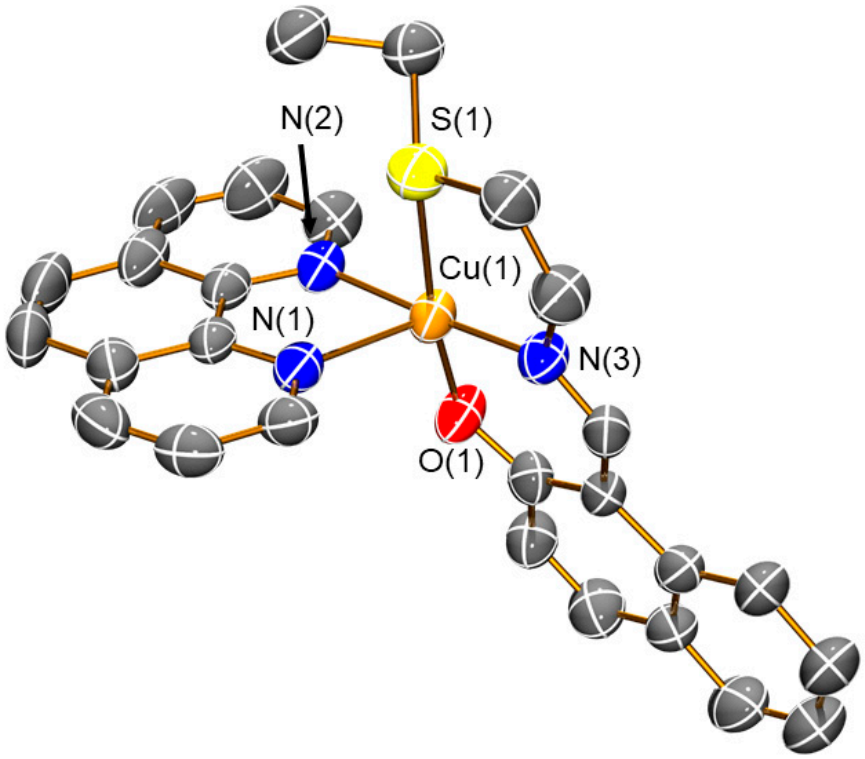

Cu(1)-S(1A)	2.50(2)	Cu(1)-N(1)	2.220(4)
Cu(1)-S(1B)	2.50(2)	Cu(1)-N(2)	2.000(4)
Cu(1)-O(1)	1.916(3)	Cu(1)-N(3)	1.915(4)
O(1)-Cu(1)-N(1)	108.4(2)	N(2)-Cu(1)-S(1A)	93.3(4)
O(1)-Cu(1)-N(2)	90.4(2)	N(2)-Cu(1)-S(1B)	91.15(13)
O(1)-Cu(1)-S(1A)	172.6(4)	N(3)-Cu(1)-O(1)	93.4(2)
O(1)-Cu(1)-S(1B)	144.42(13)	N(3)-Cu(1)-N(1)	100.4(2)
N(1)-Cu(1)S(1A)	78.6(4)	N(3)-Cu(1)-N(2)	176.2(2)
N(1)-Cu(1)-S(1B)	106.73(11)	N(3)-Cu(1)-S(1A)	82.9(4)
N(2)-Cu(1)-N(1)	78.9(2)	N(3)-Cu(1)-S(1B)	85.44(13)

Table S4. Experimentally determined LogP values for **2**-**5**.

Metal complex	LogP
2	−0.39 ± 0.06
3	−0.63 ± 0.03
4	0.02 ± 0.04
5	0.34 ± 0.03

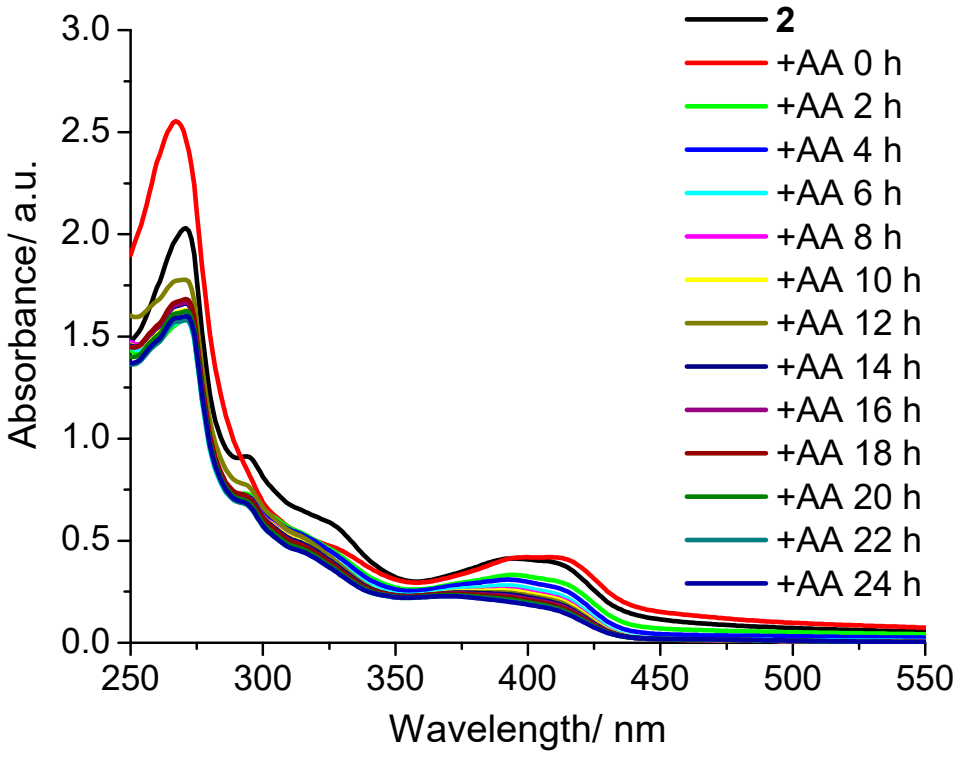

Figure S15. UV-Vis spectrum of **2** (50 μM) in the presence of ascorbic acid (500 μM) in PBS:DMSO (200:1) over the course of 24 h at 37 °C.

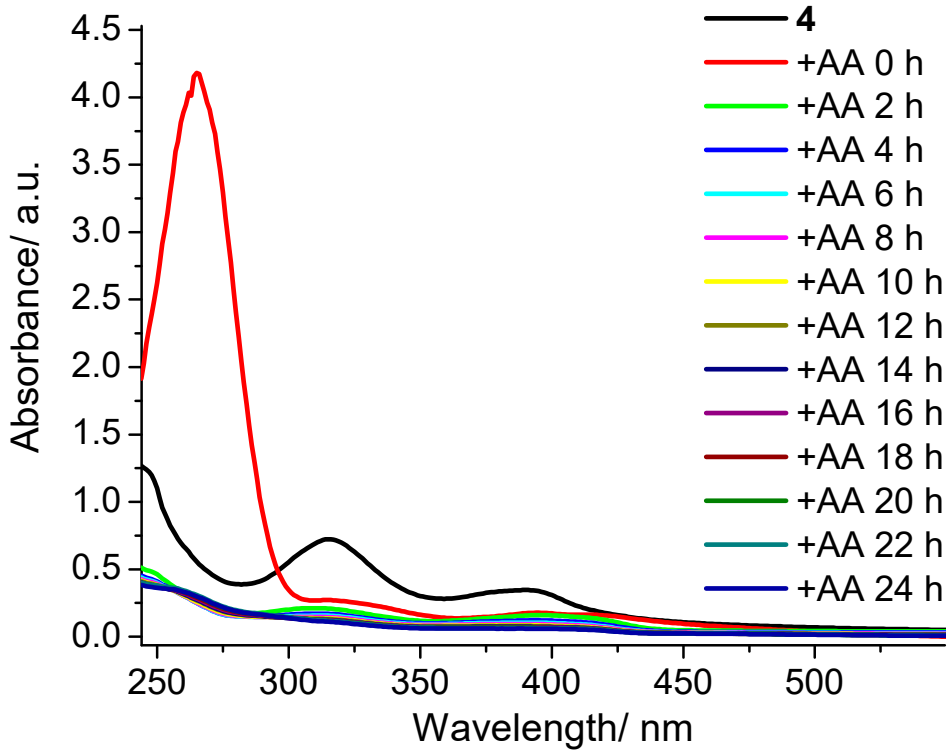

Figure S16. UV-Vis spectrum of **4** (50 μM) in the presence of ascorbic acid (500 μM) in PBS:DMSO (200:1) over the course of 24 h at 37 °C.

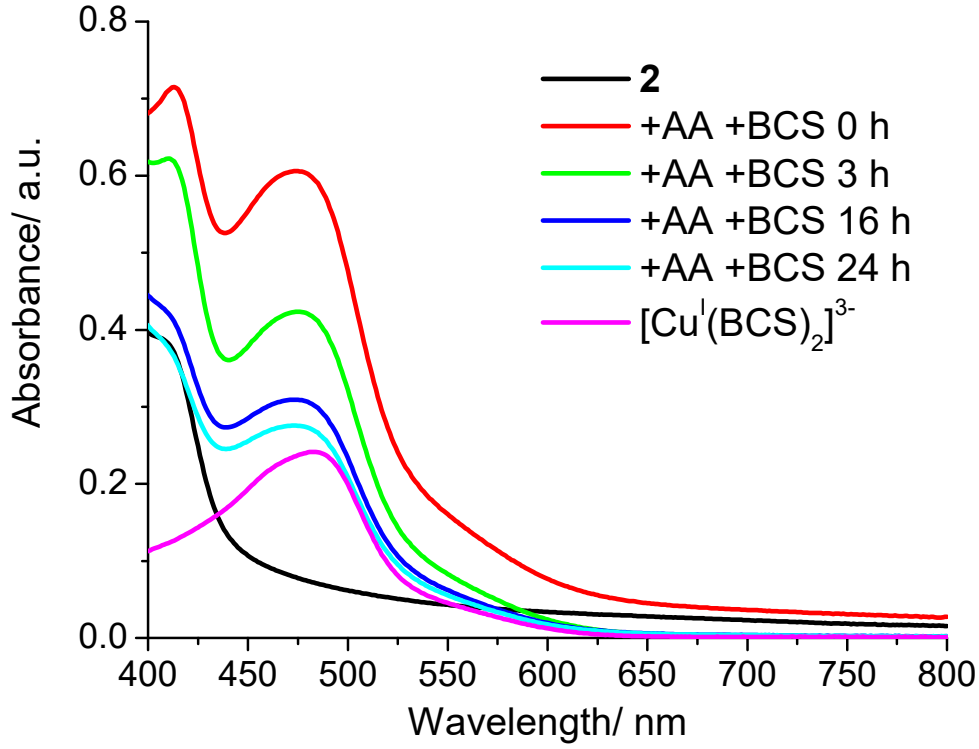

Figure S17. UV-Vis spectrum of **2** (50 μM) in the presence of ascorbic acid (500 μM) and bathocuproine disulfonate, BCS (100 μM) in PBS:DMSO (200:1) over the course of 24 h at 37 °C.

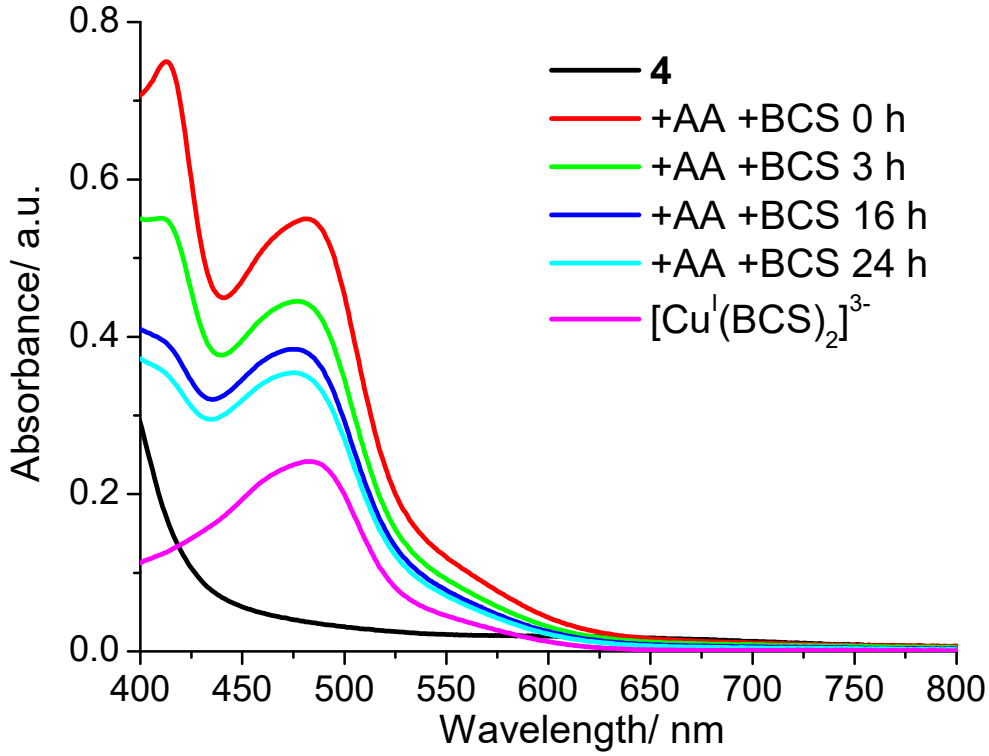

Figure S18. UV-Vis spectrum of **4** (50 μM) in the presence of ascorbic acid (500 μM) and bathocuproine disulfonate, BCS (100 μM) in PBS:DMSO (200:1) over the course of 24 h at 37 °C.

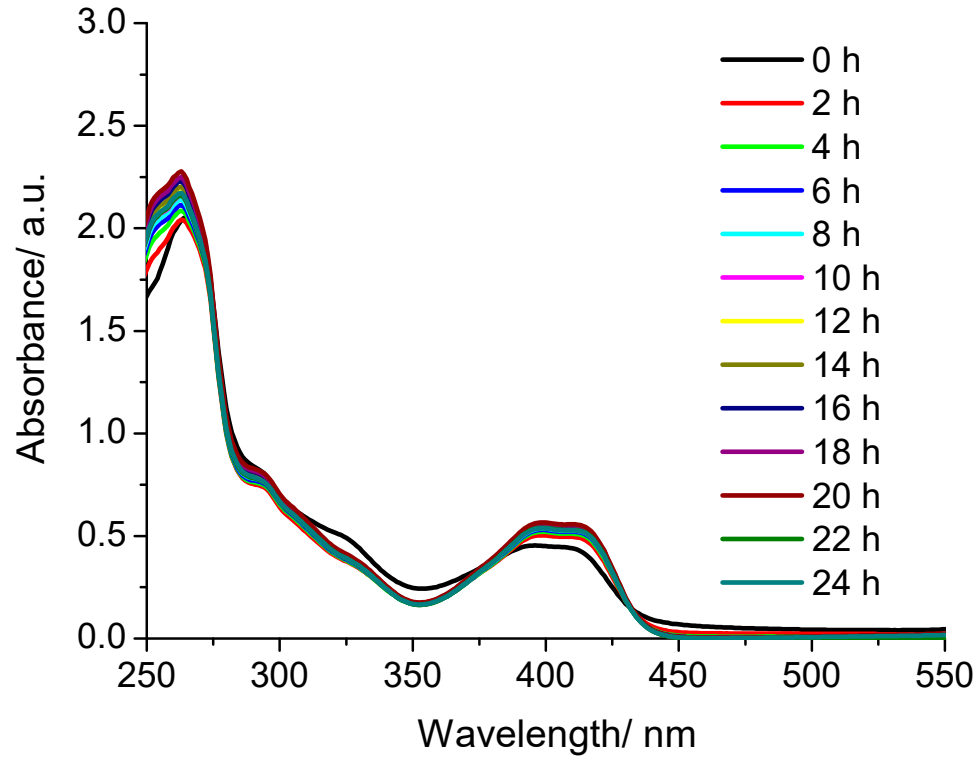

Figure S19. UV-Vis spectrum of **2** (50 μM) in mammary epithelial cell growth medium (MEGM):DMSO (200:1) over the course of 24 h at 37 °C.

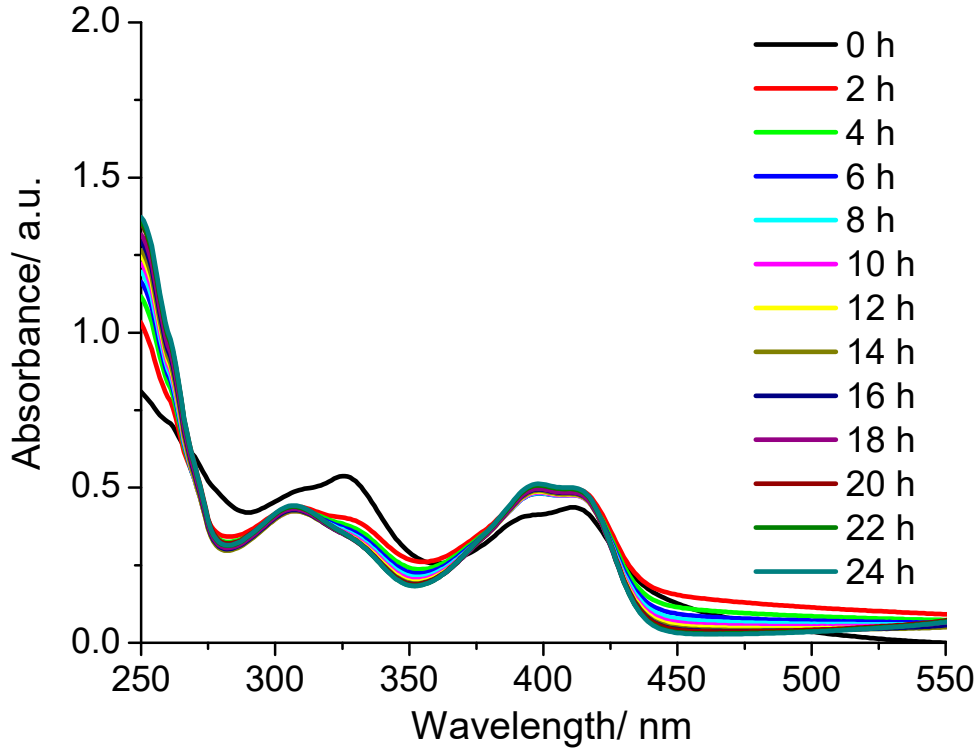

Figure S20. UV-Vis spectrum of **4** (50 μM) in mammary epithelial cell growth medium (MEGM):DMSO (200:1) over the course of 24 h at 37 °C.

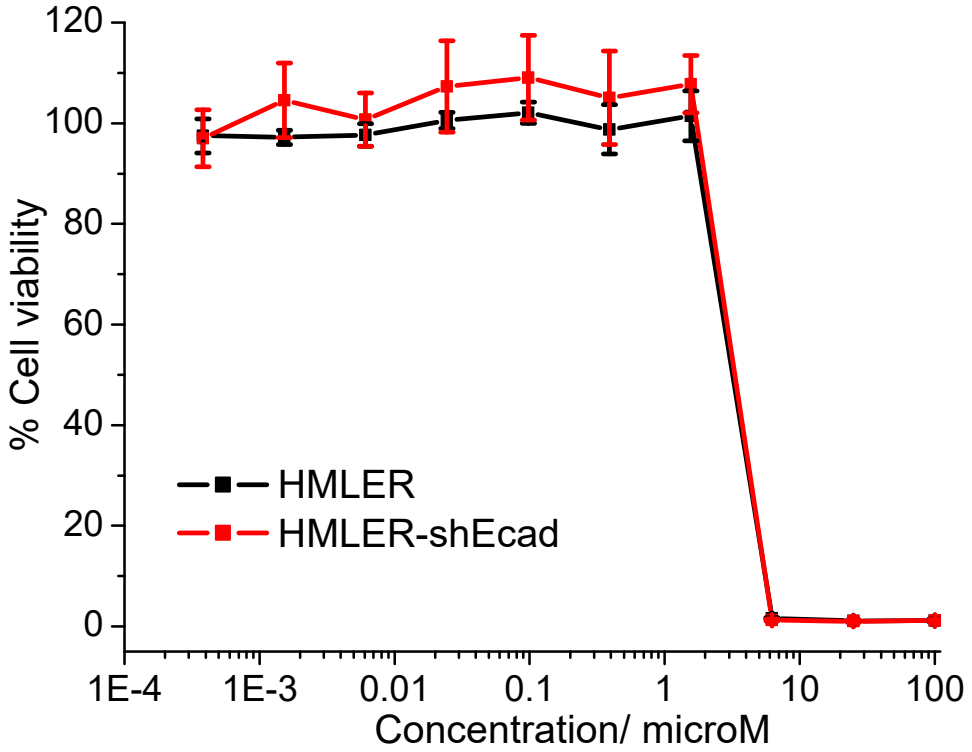

Figure S21. Representative dose-response curves for the treatment of HMLER and HMLER-shEcad cells with **2**.

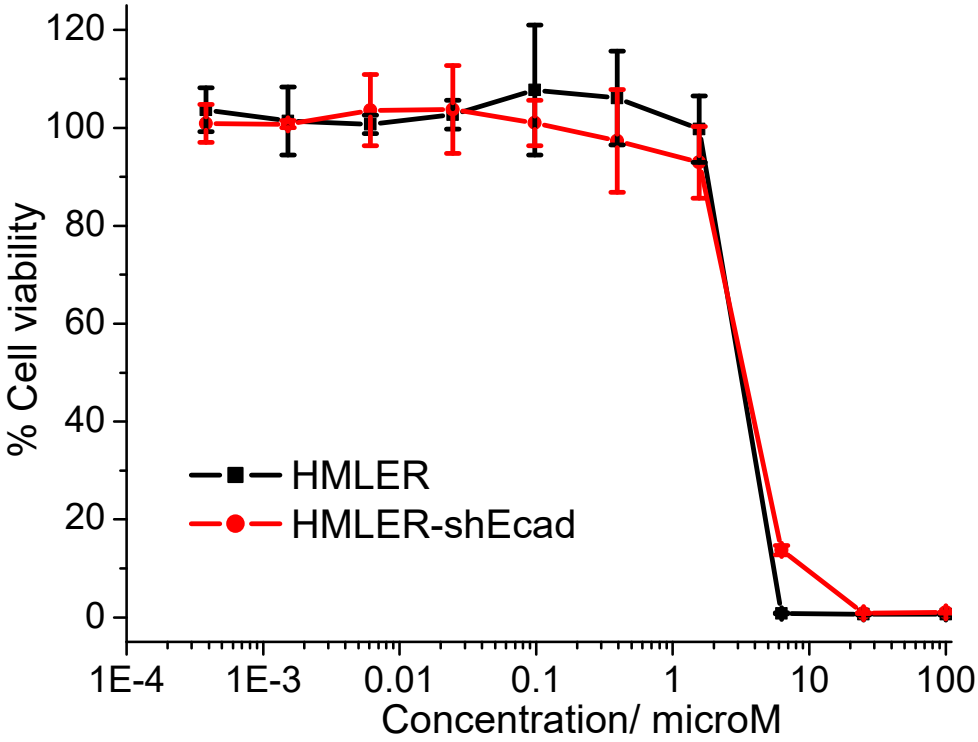

Figure S22. Representative dose-response curves for the treatment of HMLER and HMLER-shEcad cells with **3**.

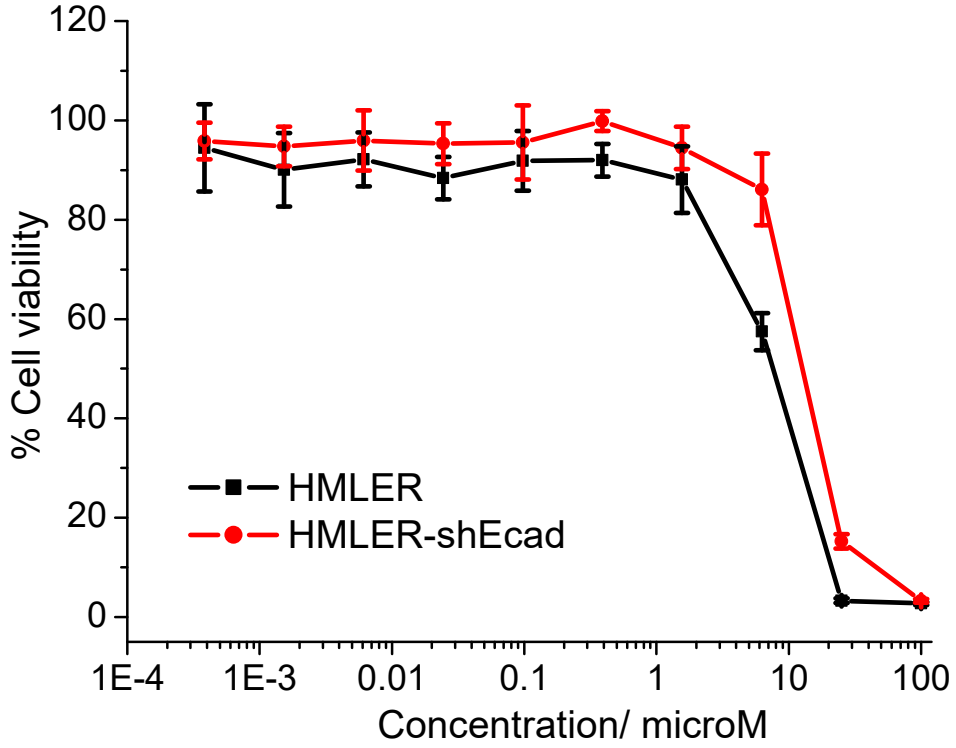

Figure S23. Representative dose-response curves for the treatment of HMLER and HMLER-shEcad cells with **4**.

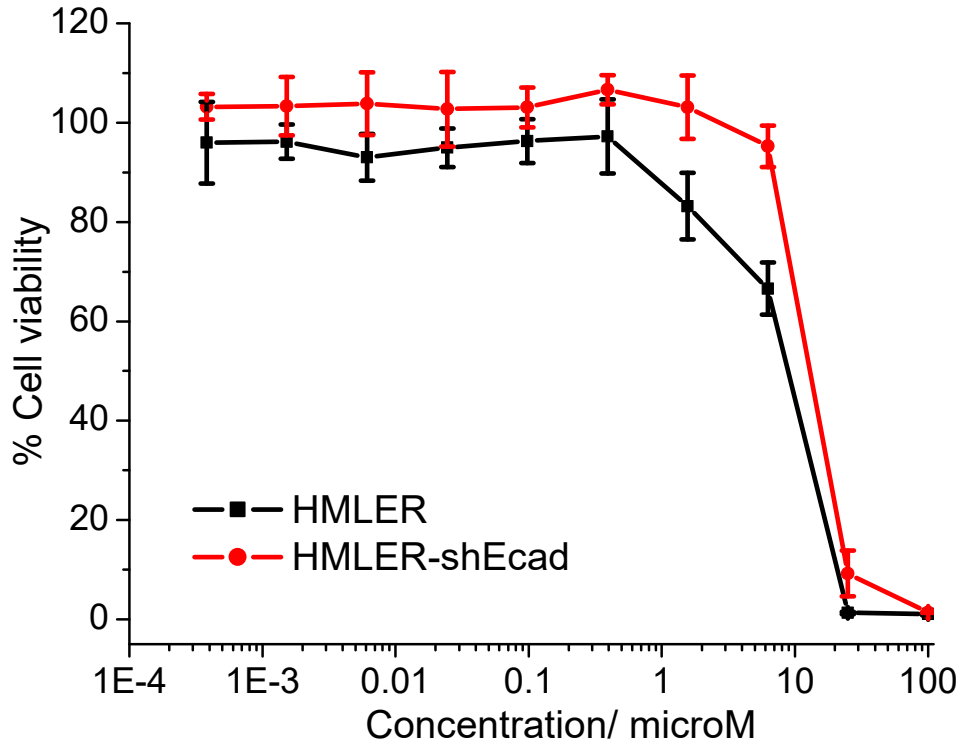

Figure S24. Representative dose-response curves for the treatment of HMLER and HMLER-shEcad cells with **5**.

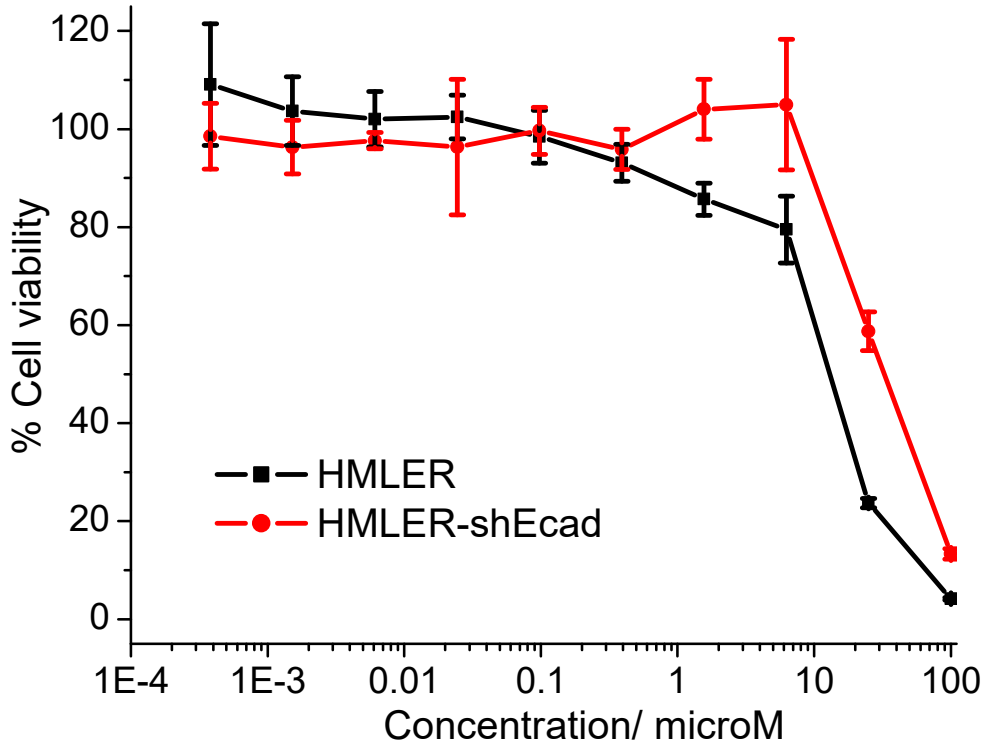

Figure S25. Representative dose-response curves for the treatment of HMLER and HMLER-shEcad cells with **L²**.

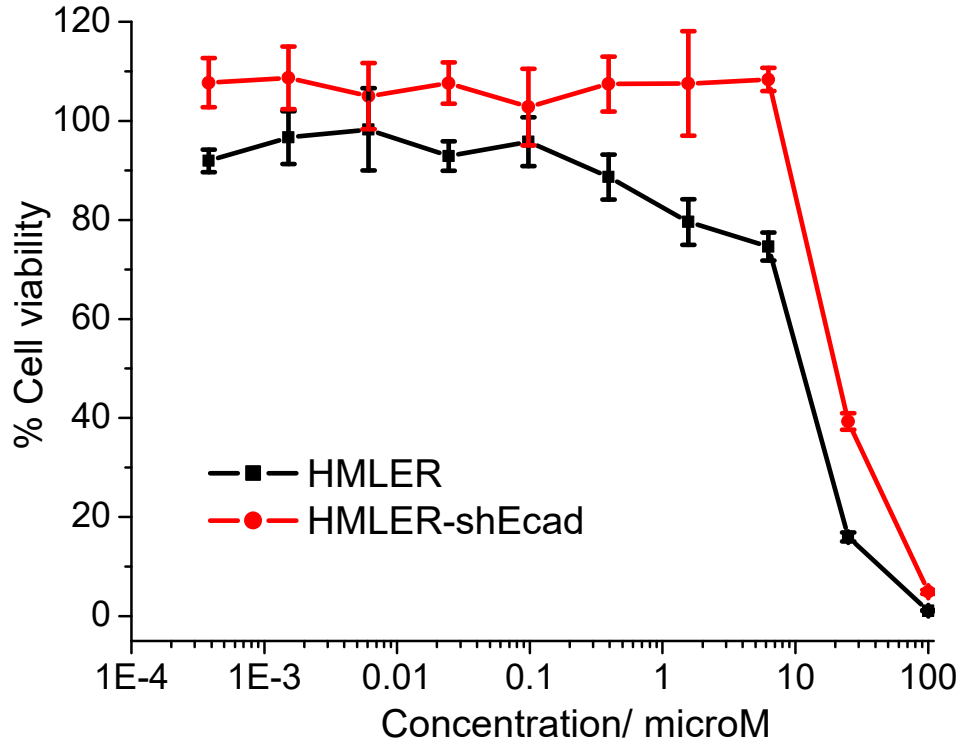

Figure S26. Representative dose-response curves for the treatment of HMLER and HMLER-shEcad cells with **L³**.

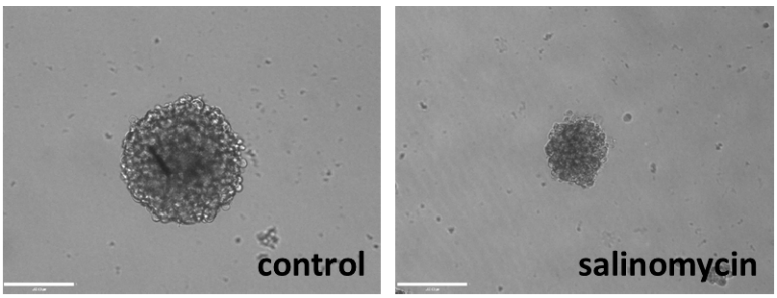

Figure S27. Bright-field images (taken using an inverted microscope) representative of untreated HMLER-shEcad mammospheres and those treated with salinomycin for 5 days at its IC_{20} values. Scale bar = 160 μm.

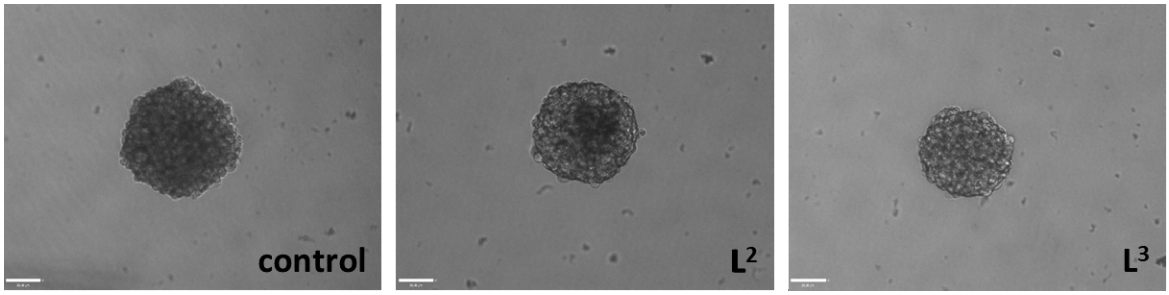

Figure S28. Bright-field images (taken using an inverted microscope) representative of untreated HMLER-shEcad mammospheres and those treated with **L²** or **L³** for 5 days at their respective IC_{20} values. Scale bar = 100 μm.

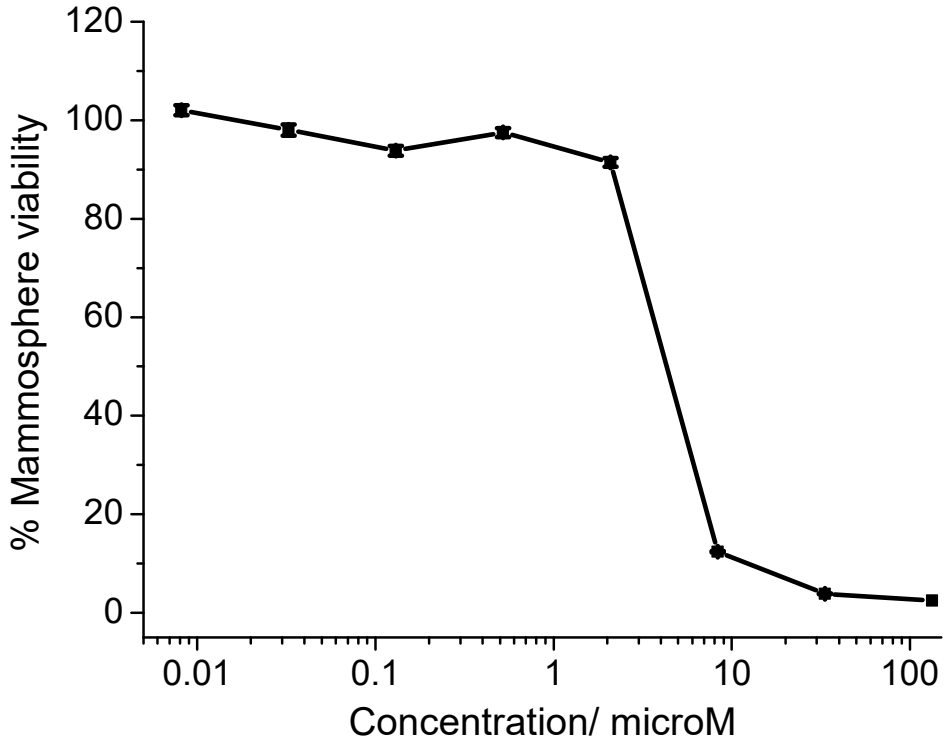

Figure S29. Representative dose-response curve for the treatment of HMLER-shEcad mammospheres with **2** after 5 days incubation.

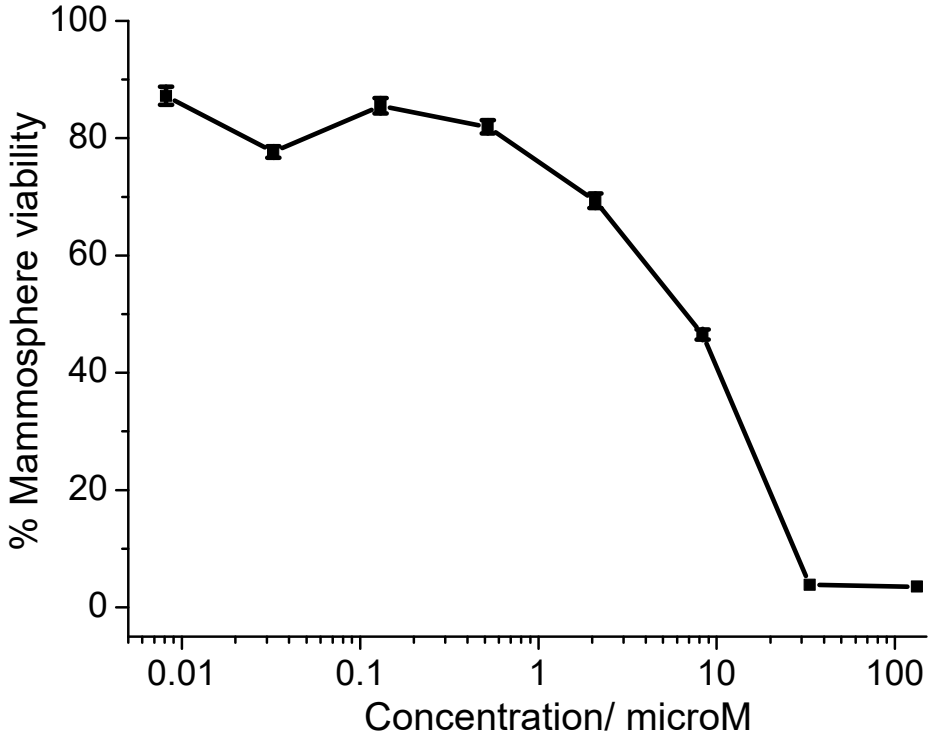

Figure S30. Representative dose-response curve for the treatment of HMLER-shEcad mammospheres with **3** after 5 days incubation.

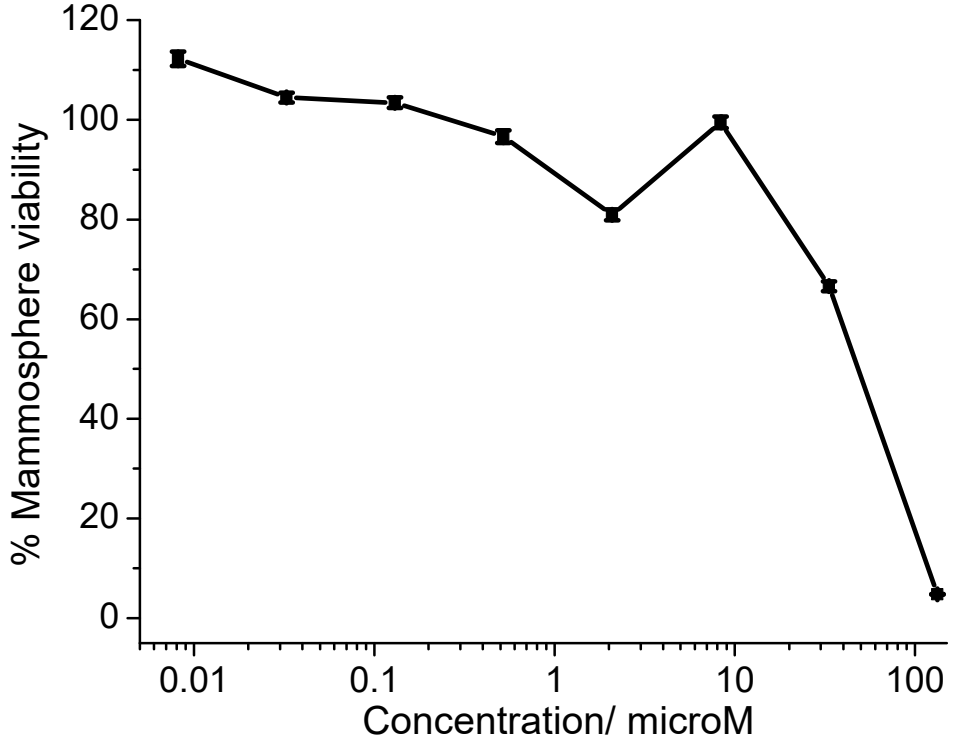

Figure S31. Representative dose-response curve for the treatment of HMLER-shEcad mammospheres with **4** after 5 days incubation.

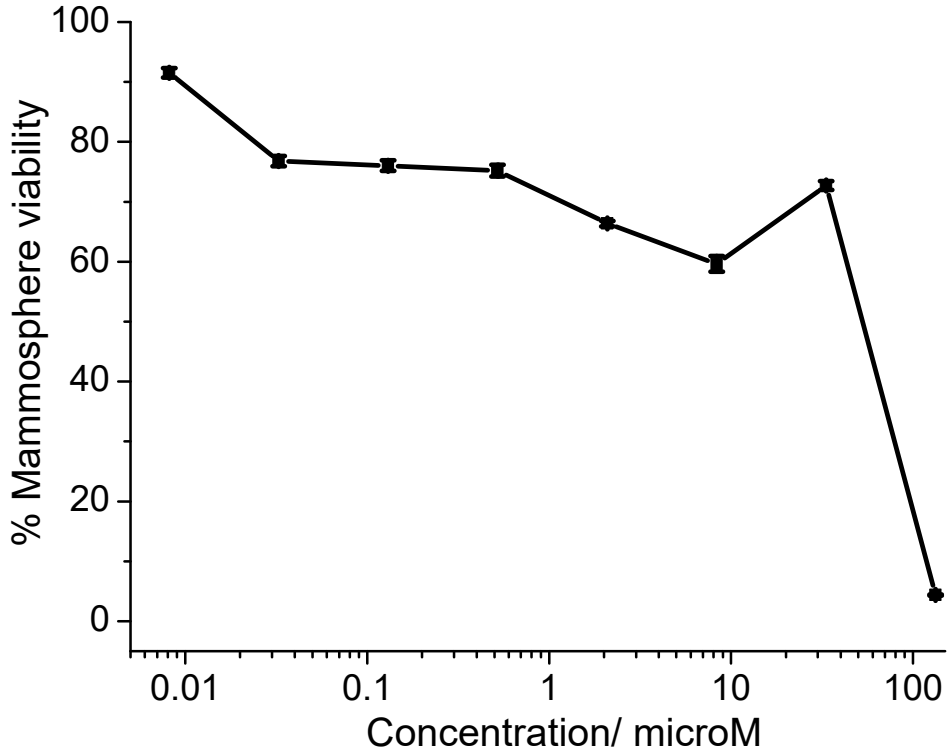

Figure S32. Representative dose-response curve for the treatment of HMLER-shEcad mammospheres with **5** after 5 days incubation.

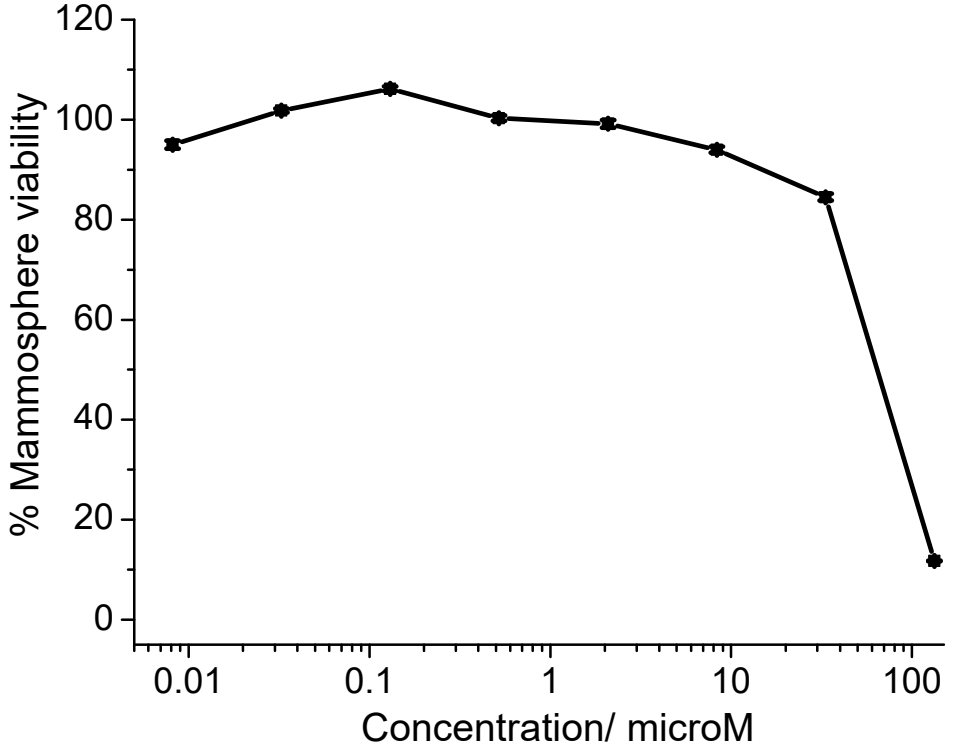

Figure S33. Representative dose-response curve for the treatment of HMLER-shEcad mammospheres with **L²** after 5 days incubation.

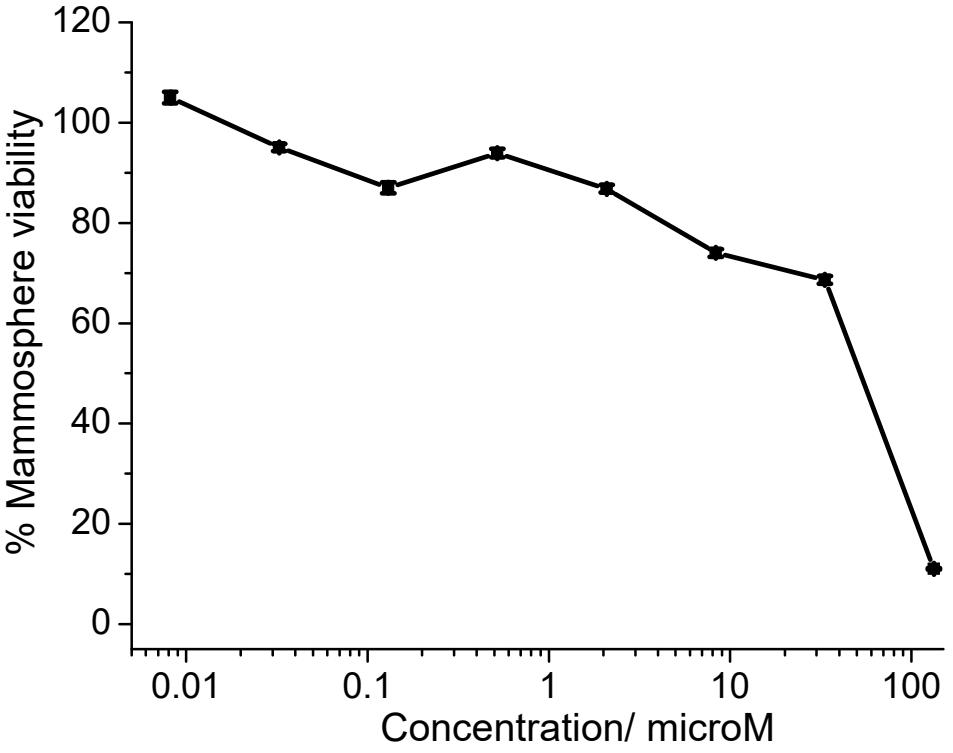

Figure S34. Representative dose-response curve for the treatment of HMLER-shEcad mammospheres with **L**[3] after 5 days incubation.

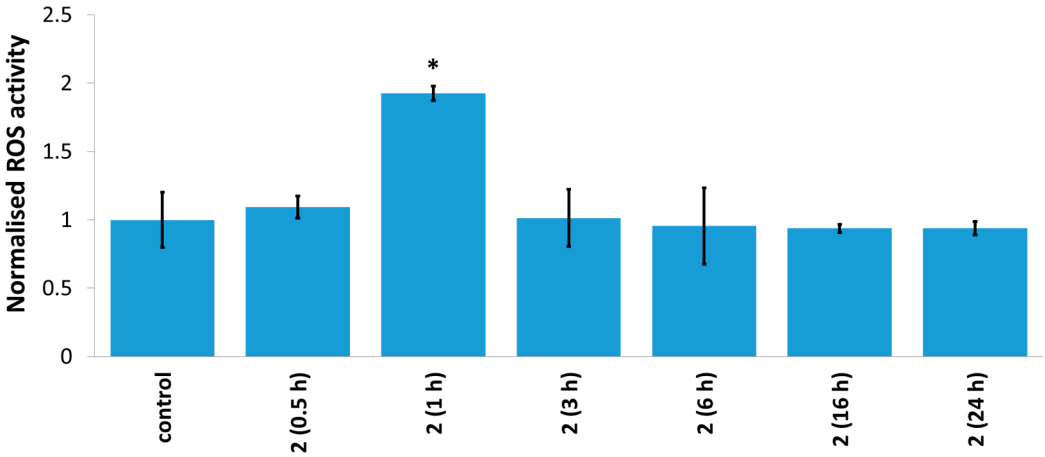

Figure S35. Normalised ROS activity in untreated HMLER-shEcad cells (control) and HMLER-shEcad cells treated with **2** (2 × IC_{50} value for 0.5, 1, 3 6, 16, and 24 h). Error bars represent standard deviations and Student *t test*, * = $p < 0.05$.

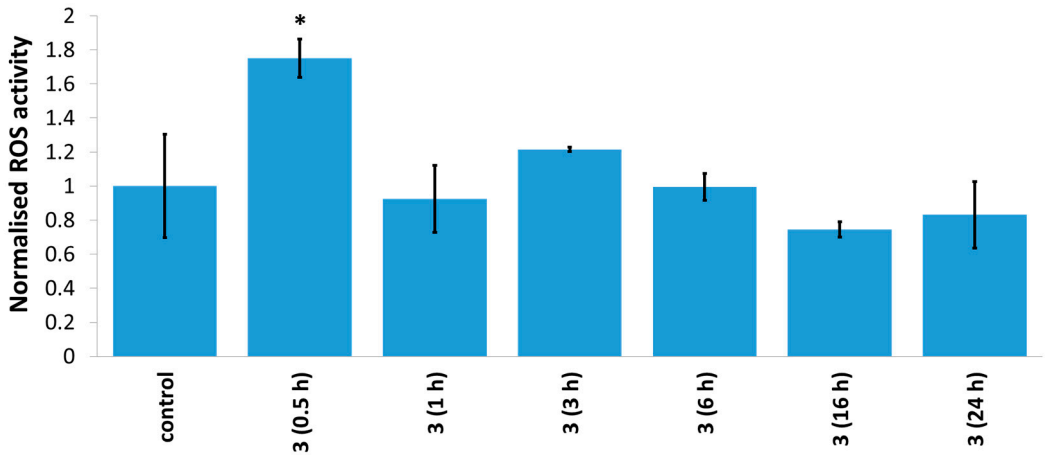

Figure S36. Normalised ROS activity in untreated HMLER-shEcad cells (control) and HMLER-shEcad cells treated with **3** (2 × IC_{50} value for 0.5, 1, 3 6, 16, and 24 h). Error bars represent standard deviations and Student *t test*, * = $p < 0.05$.

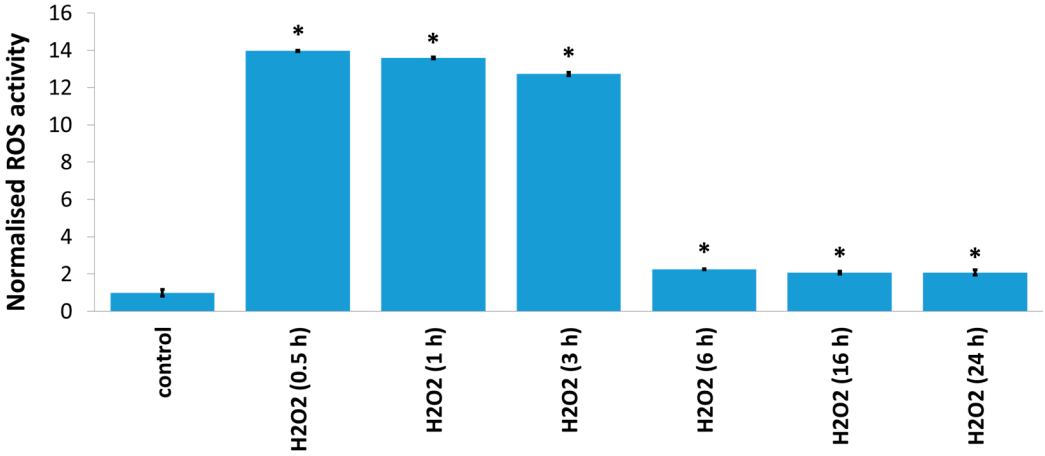

Figure S37. Normalised ROS activity in untreated HMLER-shEcad cells (control) and HMLER-shEcad cells treated with H_2O_2 (150 μM for 0.5, 1, 3 6, 16, and 24 h). Error bars represent standard deviations and Student *t test*, * = $p < 0.05$.